Journal of Luminescence 157 (2015) 69–73

Contents lists available at ScienceDirect

Journal of Luminescence

journal homepage: www.elsevier.com/locate/jlumin

Mn^{4+} emission in pyrochlore oxides

M.H. Du *

Materials Science & Technology Division, Oak Ridge, TN 37831, USA

ARTICLE INFO

Article history:
Received 10 May 2014
Received in revised form
27 June 2014
Accepted 18 August 2014
Available online 27 August 2014

Keywords:
Red phosphor
Mn^{4+}
Pyrochlore
Fluorescent lighting

ABSTRACT

Existing Mn^{4+} activated red phosphors have relatively low emission energies (or long emission wavelengths) and are therefore inefficient for general lighting. Density functional calculations are performed to study Mn^{4+} emission in rare-earth hafnate, zirconate, and stannate pyrochlore oxides ($RE_2Hf_2O_7$, $RE_2Zr_2O_7$, and $RE_2Sn_2O_7$). The results show how the different sizes of the RE^{3+} cation in these pyrochlores affect the local structure of the distorted MnO_6 octahedron, the Mn–O hybridization, and the Mn^{4+} emission energy. The Mn^{4+} emission energies of many pyrochlores are found to be higher than those currently known for Mn^{4+} doped oxides and should be closer to that of $Y_2O_3:Eu^{3+}$ (the current commercial red phosphor for fluorescent lighting). The O–Mn–O bond angle distortion in a MnO_6 octahedron is shown to play an important role in weakening Mn–O hybridization and consequently increasing the Mn^{4+} emission energy. This result shows that searching for materials that allow significant O–Mn–O bond angle distortion in a MnO_6 octahedron is an effective approach to find new Mn^{4+} activated red phosphors with potential to replace the relatively expensive $Y_2O_3:Eu^{3+}$ phosphor.
© 2014 Elsevier B.V. All rights reserved.

1. Introduction

Mn^{4+} can activate red emission in many materials [1,2]. The Mn^{4+} emission wavelengths in some fluorides [3–6] are close to that of $Y_2O_3:Eu^{3+}$, which is the current commercial red phosphor used in fluorescent lighting. (The Mn^{4+} emission wavelength in Na_2SiF_6 is 617 nm [5], compared with 611 nm for $Y_2O_3:Eu^{3+}$.) Therefore, Mn^{4+} has the potential to replace the more expensive Eu-activated red phosphors. However, the fluorides are not stable in the mercury vapor environment, which is present in fluorescent lamps. Many Mn^{4+} activated oxides are stable in mercury environment but their emission wavelengths are relatively too long compared to that of $Y_2O_3:Eu^{3+}$. The shortest reported Mn^{4+} emission wavelength in oxides is 648 nm for $Y_2Sn_2O_7$ [7]. It is important to note that human eye sensitivity to red light decreases rapidly when the emission wavelength goes above 611 nm (by more than 60% from 611 to 648 nm). Hence, the currently known Mn^{4+} activated oxide phosphors are inefficient for general lighting.

Mn can assume many oxidation states, such as 2+, 3+, 4+, and 5+, depending on the chemical environment of the Mn ion. An Mn ion usually assumes the 4+ oxidation state when it is located on an octahedral site in solids because the octahedral crystal field creates a large energy gap between the occupied t_{2g} and the empty e_g orbitals in Mn^{4+} [2]. The emission spectrum of Mn^{4+} typically shows a sharp line corresponding to the $^2E_g \rightarrow {}^4A_{2g}$ transition. The variation in the Mn^{4+} emission energies in different materials is attributed to different hybridization strength between Mn^{4+} and its ligands [1,2,8]. Weaker Mn^{4+}-ligand hybridization usually lead to higher emission energy (or shorter emission wavelength). Substitutional Mn^{4+} on large cation sites usually forms long Mn^{4+}-ligand bond, resulting in relatively weak hybridization and high emission energy. A recent study further shows that bond angle distortion around the Mn octahetral site significantly decreases the Mn^{4+}-ligand hybridization, thereby increasing the emission energy [2]. This explains, for instance, why the Mn^{4+} emission energies in pyrochlore oxides (with significant bond angle distortion in MnO_6 octahedra) are generally higher than those in perovskite oxides (with no or small bond angle distortion in MnO_6 octahedra). $Y_2Sn_2O_7$, which is the oxide with shortest reported Mn^{4+} emission wavelength [7], is a pyrochlore oxide.

Pyrochlore oxides are a large family of oxides with general formula of $A_2B_2O_7$ (space group Fd-3m) [9]. Fig. 1 shows the structure of rare-earth pyrochlore oxides ($A_2^{3+}B_2^{4+}O_7^{2-}$), where the A-site contains the large rare-earth cations (RE^{3+}) and the B-site consists of smaller (e.g., Sn^{4+}, Zr^{4+}, Hf^{4+}), higher-valence cations. The larger RE^{3+} cations are eight-fold coordinated with oxygen and located within a distorted cubic polyhedron. The smaller B^{4+} cation is six-fold-coordinated with oxygen and located in a distorted octahedron, which is illustrated in Fig. 1.

This work employs density functional calculations [10] to show how the different sizes of the RE^{3+} cation in rare-earth hafnate, zirconate, and stannate pyrochlore oxides ($RE_2Hf_2O_7$, $RE_2Zr_2O_7$, and $RE_2Sn_2O_7$) affect the local structure of the distorted MnO_6 octahedron, the Mn–O hybridization, and the Mn^{4+} emission

* Tel.: +1 8655766711.
E-mail address: mhdu@ornl.gov

http://dx.doi.org/10.1016/j.jlumin.2014.08.038
0022-2313/© 2014 Elsevier B.V. All rights reserved.

energy. There are many rare-earth pyrochlores. Here, only those with large-sized tetravalent ions (i.e., Hf^{4+}, Zr^{4+}, and Sn^{4+}) are chosen since these ions, when substituted by Mn^{4+}, allow relatively long Mn–O bond length, which results in weak Mn–O hybridization and high Mn^{4+} emission energy. (The ionic radii of Hf^{4+}, Zr^{4+}, and Sn^{4+} are 0.85 Å, 0.86 Å, and 0.83 Å, respectively, much larger than that of Mn^{4+}, which is 0.67 Å [11].) The emission energies of a large number of Mn^{4+} doped rare-earth pyrochlores are found to be higher than those currently known for Mn^{4+} doped oxides and should be closer to that of Y_2O_3:Eu^{3+}.

2. Computational details

In this work, density functional theory (DFT) with standard Perdew–Burke–Ernzerhof (PBE) [12] is used to study the Mn^{4+} emission in rare-earth pyrochlore oxides. Since the $^2E_g \rightarrow {}^4A_{2g}$ emission at Mn^{4+} involves only a spin flip, the Mn^{4+} emission energy is calculated by taking the energy difference between the low- and the high-spin states of Mn^{4+}:

$$\Delta E_{em} = E(1\mu_B) - E(3\mu_B), \quad (1)$$

where $E(1\mu_B)$ and $E(3\mu_B)$ are the total energies of structurally relaxed low-spin ($1\mu_B$) and high-spin ($3\mu_B$) states of Mn^{4+} [2].

DFT is a ground-state single-particle theory, which in principle is incapable of calculating the transition energy between multi-electronic states. The calculated Mn^{4+} emission energies based on DFT–PBE method have been found to be significantly lower than those measured experimentally, as expected [2]. However, PBE calculations can efficiently screen a large number of materials. More importantly, PBE calculations of a large number of oxide and fluoride hosts have been shown to produce a trend of Mn^{4+} emission energies consistent with the experimental results (see Ref. [2] for details). The reason is that the variation of the Mn^{4+} emission energy in different hosts is caused by the different Mn-ligand hybridization strengths [1,2,8], which can be distinguished by DFT–PBE calculations. Therefore, although calculating Eq. (1) using the DFT–PBE method cannot give the correct Mn^{4+} emission energy, it produces a correct trend, which can be used for predicting Mn^{4+} emission energies in new oxide materials. For example, one can identify new Mn^{4+} doped oxides with emission energies that are higher than those currently known and closer to that of Y_2O_3:Eu^{3+}, as has been done in Ref. [2].

All the calculations were performed using the VASP codes [13, 14]. The electron–ion interactions were described using projector augmented wave potentials [15,13]. The 4f electrons of the rare-earth cations are frozen in the core because the 4f states are highly localized and have little interaction with valence states. The valence wavefunctions were expanded in a plane-wave basis with cut-off energy of 400 eV. All the atoms were relaxed to minimize the Feynman–Hellmann forces to below 0.02 eV/Å. The previously calculated structures of rare-earth titanate pyrochlores, which

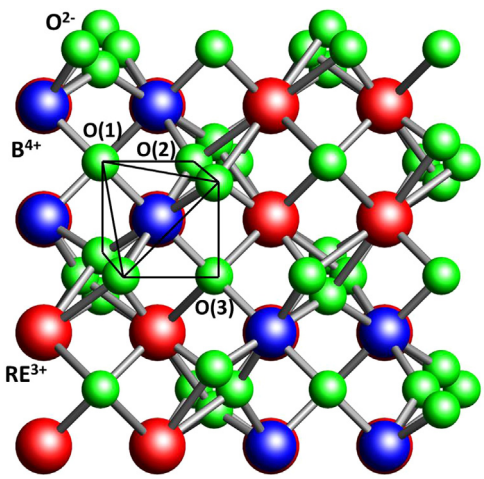

Fig. 1. Structure of rare-earth pyrochlore oxides ($RE_2B_2O_7$).

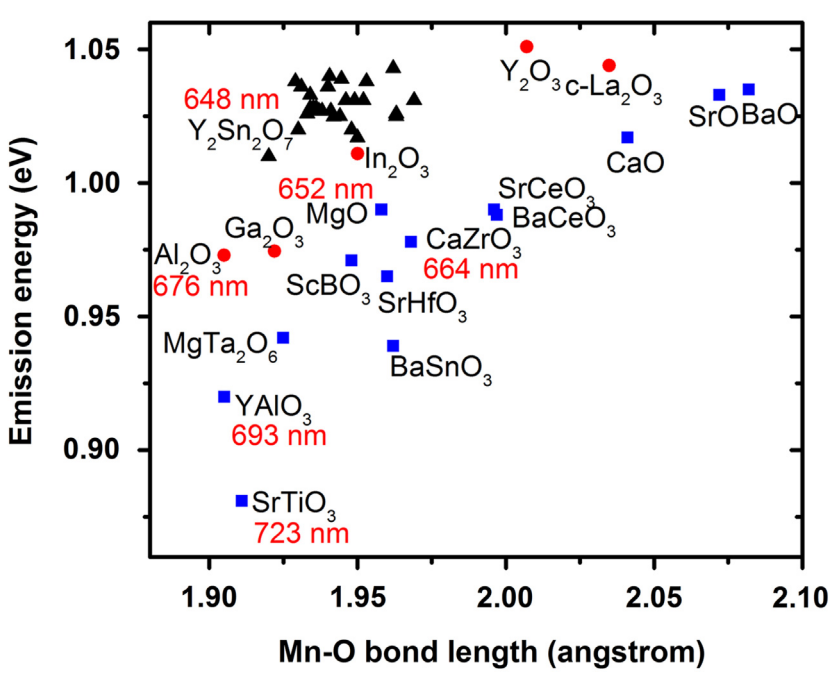

Fig. 2. PBE-calculated Mn^{4+} emission energies as functions of Mn–O bond length for oxides. The Mn–O bond length is the average over the six Mn–O bond lengths in the MnO_6 octahedron. The experimental values are shown (in red) wherever available (i.e., for $SrTiO_3$, $YAlO_3$, Al_2O_3, $CaZrO_3$, MgO, and $Y_2Sn_2O_7$). Some of the materials shown in the figure have no or small (< 2°) O–Mn–O bond angle distortion (blue squares) while some other have relatively large (> 4°) O–Mn–O bond angle distortion (red circles and black triangles). Black triangles represent pyrochlore oxides, which are shown in more details in Fig. 3. (For interpretation of the references to color in this figure legend, the reader is referred to the web version of this article.)

were obtained by employing the same methodologies outlined above, showed excellent agreement with experimental results [16]. Heyd–Scuseria–Ernzerhof (HSE06) hybrid functionals [17,18] were also used for calculating band gaps of selected materials.

3. Results and discussion

Fig. 2 shows the PBE-calculated Mn^{4+} emission energies for a large number of oxide hosts. The experimentally measured emission energies are shown wherever available. Some of the results in Fig. 2 have been published previously [2]. They are shown here along with the new results on pyrochlores to demonstrate some general trends. It can be seen that the calculated Mn^{4+} emission energies for oxide hosts with diverse crystal structures [i.e., $SrTiO_3$ (cubic perovskite), $YAlO_3$ (orthorhombic perovskite), Al_2O_3 (corundum), $CaZrO_3$ (orthorhombic perovskite), MgO (rock salt), and $Y_2Sn_2O_7$ (pyrochlore)] exhibit a correct trend compared with the experimental results. (A detailed comparison between calculated and measured Mn^{4+} emission energies can be found in Ref. [2].) This demonstrates that the DFT–PBE calculation is capable of distinguishing different Mn–O hybridization strength in oxides of diverse crystal structures and producing a correct Mn^{4+} emission energy trend. The Mn^{4+} emission energy generally increases with increasing Mn–O bond length (due to the decreasing Mn–O hybridization strength). For example, this is the case for Mn^{4+}

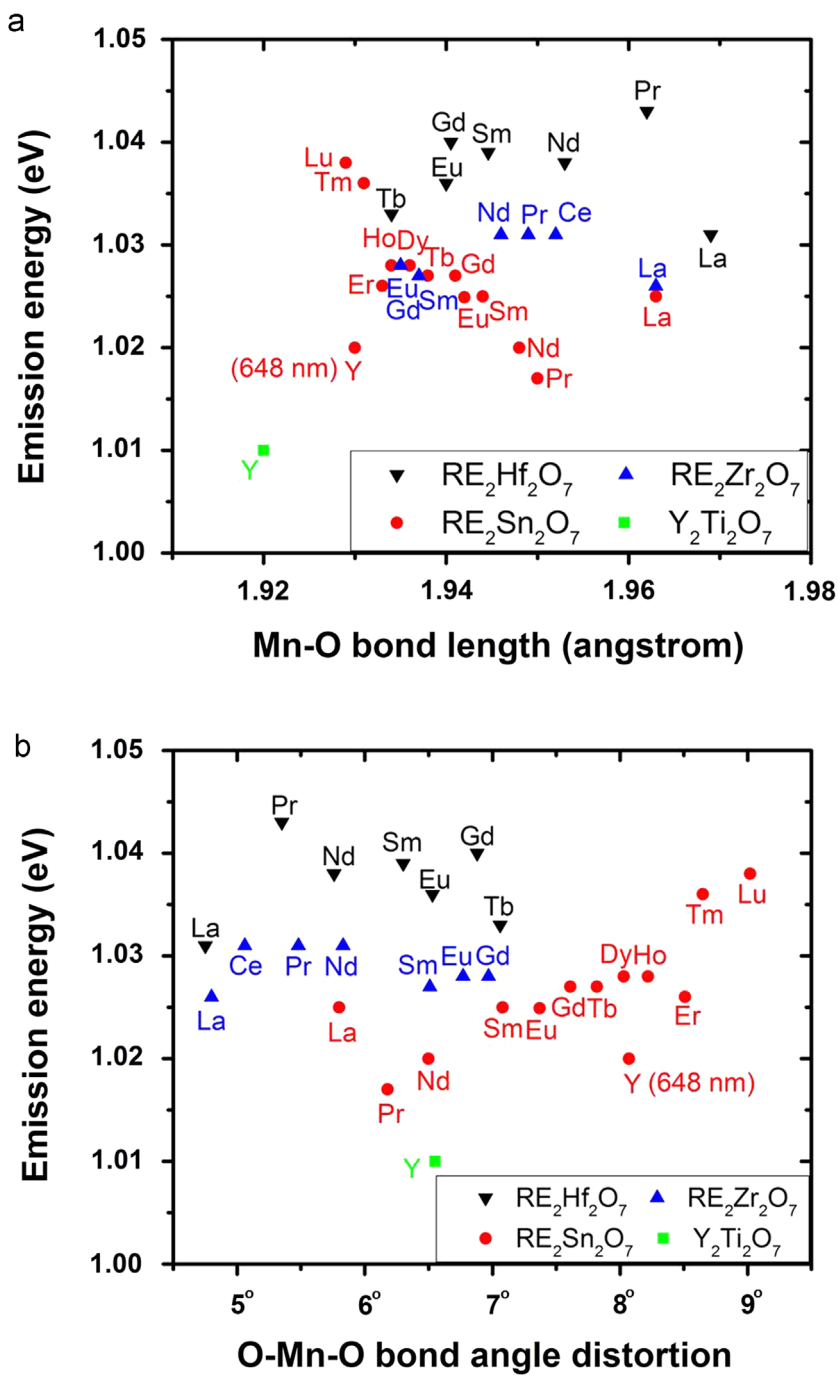

Fig. 3. PBE-calculated Mn^{4+} emission energies for rare-earth pyrochlores as functions of Mn–O bond length (a) and O–Mn–O bond angle distortion (b). The calculated Mn–O bond lengths and Mn^{4+} emission energies for $Eu_2Zr_2O_7$ and $Gd_2Zr_2O_7$ are nearly the same and are therefore represented by one data point in (a).

emission in oxides of perovskite (e.g., $SrTiO_3$, $BaSnO_3$, $SrHfO_3$, $CaZrO_3$, $SrCeO_3$, and $BaCeO_3$) and rock salt (i.e., MgO, CaO, SrO, and BaO) structures. However, such trend is less clear for pyrochlores, which have relatively large O–Mn–O bond angle distortion in MnO_6 octahetra [2]. The results for pyrochlores ($RE_2Hf_2O_7$, $RE_2Zr_2O_7$, $RE_2Sn_2O_7$, and $Y_2Ti_2O_7$) are represented by black triangles in Fig. 2. The pyrochlores have higher Mn^{4+} emission energies than other oxides with similar Mn–O bond length as shown in Fig. 2, which shows the importance of O–Mn–O bond angle distortion in reducing the Mn–O hybridization strength and increasing the Mn^{4+} emission energy.

The part of Fig. 2 that shows Mn^{4+} emission energies of pyrochlores is enlarged in Fig. 3 to show details. For rare-earth stannate pyrochlores, the pyrochlore structure is stable for nearly the entire lanthanide series plus yttrium. $Ce_2Sn_2O_7$ has not been reported perhaps because Ce^{3+} can easily be oxidized to form Ce^{4+}. For zirconate and hafnate pyrochlores, the pyrochlore structure is stable for large-sized RE^{3+} cations. The stability of the ordered pyrochlore structure ($A_2B_2O_7$) depends to the cation ionic radius ratio (r_A/r_B). The ionic radii of Sn^{4+}, Zr^{4+}, and Hf^{4+} are 0.83, 0.86, and 0.85 Å, [11] respectively, which are quite close to each other. The ionic radius of the trivalent lanthanides decreases with successive addition of 4f electrons. The ionic radii of RE^{3+} are 1.159 (Y^{3+}), 1.172 (La^{3+}), 1.15 (Ce^{3+}), 1.13 (Pr^{3+}), 1.219 (Sm^{3+}), 1.206 (Eu^{3+}), 1.193 (Gd^{3+}), 1.180 (Tb^{3+}), 1.167 (Dy^{3+}), 1.155 (Ho^{3+}), 1.144 (Er^{3+}), 1.134 (Tm^{3+}), 1.125 (Yb^{3+}), and 1.117 (Lu^{3+}) [11]. If r_A/r_B is too small (which is the case for zirconate and hafnate pyrochlores with small RE^{3+} cations), the pyrochclore structure becomes disordered and unstable and is transformed into the defected-fluoride structure [19,20]. If r_A/r_B is too large (which is the case for titanate pyrochlores with large RE^{3+} cations), a monoclinic structure (space group $P2_1$ (No. 4)) is formed [16]. The rare-earth hafnate, zirconate, and stannate pyrochlores that have been reported in the literature as stable at room temperature are considered in Fig. 3. Yb compounds are not studied due to the lack of a good Yb^{3+} pseudopotential.

The six B–O bond lengths in the distorted BO_6 octahedron are equal to each other whereas the O–B–O bond angles deviate from 90° to $90^\circ \pm \Delta\theta$ (e.g., the O(1)–B–O(2) and the O(2)–B–O(3) bond angles in Fig. 1 are $90^\circ + \Delta\theta$ and $90^\circ - \Delta\theta$, respectively). Increasing the size of the RE^{3+} cation leads to increased B–O bond length and decreased O–B–O bond angle distortion (i.e., smaller $\Delta\theta$). When a B cation is substituted by a Mn cation, the increased Mn–O bond length and the decreased O–Mn–O bond angle as the result of increasing the size of the RE^{3+} cation have the opposite effects, i.e., the former weakens the Mn–O hybridization whereas the latter enhances it [2]. This results in the lack of a clear trend in the Mn^{4+} emission energy as a function of Mn–O bond length or O–Mn–O bond angle distortion in zirconate and hafnate pyrochlores, as shown in Fig. 3(a) and (b).

For stannate pyrochlores, as RE^{3+} cation size decreases from La^{3+} to Lu^{3+}, Mn^{4+} emission energies exhibit a rising trend while the Mn–O bond length decreases (which enhances Mn–O hybridization) and the O–Mn–O bond angle distortion increases (which weakens Mn–O hybridization). Since the Mn^{4+} emission energy increases with weakening Mn–O hybridization, the results in Fig. 3 demonstrate that, for rare-earth stannate pyrochlores, the increase of the O–Mn–O bond angle distortion has a stronger effect on Mn–O hybridization than the decrease of the Mn–O bond length.

The highest measured Mn^{4+} emission energy for oxides is 648 nm for $Y_2Sn_2O_7$ [7]. Fig. 3 shows that many Mn^{4+} doped rare-earth pyrochlores exhibit higher emission energies that are closer to that of Y_2O_3:Eu^{3+}, the current commercial red phosphor. The hafnate and zirconate pyrochlores have larger band gaps than those of stannate pyrochlores. The band gaps of $La_2Hf_2O_7$, $La_2Zr_2O_7$, and $La_2Sn_2O_7$ obtained from HSE calculations are 6.12 eV, 5.68 eV, and 4.49 eV, respectively. Having a phosphor with a band gap larger than the main emission energy of mercury ion (4.88 eV) is important for use in fluorescent lamps because it can avoid across-band-gap excitation of the phosphor (by UV emission from mercury), which can cause non-radiative recombination at defects and lower quantum efficiency of the phosphor. Some rare-earth elements, e.g., La, Ce, Pr, Sm, and Gd, are substantially less expensive than Eu. The pyrochlores that contain these rare-earth elements are interesting for research on low-cost red phosphors used for fluorescent lighting.

The results shown in Figs. 2 and 3, highlight the importance of O–Mn–O bond angle distortion (in a MnO_6 octahedron) in weakening the Mn–O hybridization and consequently in increasing the Mn^{4+} emission energy. Among all the oxides shown in Fig. 2 with tetravalent cation sites for Mn^{4+} substitution, $SrCeO_3$ and $BaCeO_3$ have the largest tetravalent cation, i.e., Ce^{4+}, which has an ionic radius of 1.01 Å, much larger than those of Hf^{4+} (0.85 Å), Zr^{4+} (0.86 Å), Sn^{4+} (0.83 Å), and Ti^{4+}(0.745 Å) [11]. As a result, the Mn–O bond lengths in $SrCeO_3$ and $BaCeO_3$ are longer than those in hafnate, zirconate, stannate, and titanate pyrochlores as shown in Fig. 2. However, the Mn^{4+} emission energies of all these pyrochlores are higher than those of $SrCeO_3$ and $BaCeO_3$ with perovskite structures because the O–Mn–O bond angle distortion in pyrochlores is much larger than that in perovskites. This result demonstrates that searching for materials that allow significant O–Mn–O bond angle distortion in a MnO_6 octahedron is an effective approach to find new Mn^{4+} activated red phosphors with higher emission energies that are closer to that of Y_2O_3:Eu^{3+}.

4. Conclusions

DFT–PBE calculations are performed to calculate the Mn^{4+} emission energies for a large number of rare-earth hafnate, zirconate, and stannate pyrochlore oxides ($RE_2Hf_2O_7$, $RE_2Zr_2O_7$, and $RE_2Sn_2O_7$). Decreasing the RE^{3+} size from La^{3+} to Lu^{3+} decreases the Mn–O bond length (which enhances the Mn–O hybridization) and increases the O–Mn–O bond angle distortion in MnO_6 octahetra (which weakens the Mn–O hybridization). Since Mn^{4+} emission energy increases with decreasing Mn–O hybridization strength, the interplay between the Mn–O bond length and the O–Mn–O bond angle determines the Mn^{4+} emission energy in pyrochlores. The calculations show that the O–Mn–O bond angle distortion has a strong impact on the Mn^{4+} emission energy and, in particular, it plays a dominant role in determining the emission energy for stannate pyrochlores. The Mn^{4+} emission energies of a large number of pyrochlores are found to be higher than those currently known for Mn^{4+} doped oxides and should be closer to that of Y_2O_3:Eu^{3+} (the current commercial red phosphor for fluorescent lighting).

Acknowledgments

The author is grateful for the useful discussion with L. A. Boatner, S. A. Payne, and David J. Singh. This work is supported by the Critical Materials Institute, an Energy Innovation Hub funded by the U.S. Department of Energy, Office of Energy Efficiency and Renewable Energy, Advanced Manufacturing Office.

References

[1] M.G. Brik, A.M. Srivastava, J. Lumin. 133 (2013) 69.
[2] M.H. Du, J. Mater. Chem. C 2 (2014) 2475.
[3] T. Takahashi, S. Adachi, J. Electrochem. Soc. 155 (2008) E183.
[4] T. Arai, S. Adachi, Jpn. J. Appl. Phys. 50 (2011) 092401.
[5] Y.K. Xu, S. Adachi, J. Appl. Phys. 105 (2009) 013525.

[6] Y. Arai, S. Adachi, J. Lumin. 131 (2011) 2652.
[7] M.G. Brik, A.M. Srivastava, Opt. Mater. 35 (2013) 1251.
[8] M.G. Brik, A.M. Srivastava, ECS J. Solid State Sci. Technol. 2 (2013) R148.
[9] M.A. Subramanian, G. Aravamudan, G.V. Subba Rao, Prog. Solid State Chem. 15 (1983) 55.
[10] W. Kohn, L.J. Sham, Phys. Rev. 140 (1965) A1133.
[11] R.D. Shannon, Acta Crystallogr. A32 (1976) 751.
[12] J.P. Perdew, K. Burke, M. Ernzerhof, Phys. Rev. Lett. 77 (1996) 3865.
[13] G. Kresse, J. Furthmüller, Phys. Rev. B 54 (1996) 11169.
[14] G. Kresse, D. Joubert, Phys. Rev. B 59 (1999) 1758.
[15] P.E. Blöchl, Phys. Rev. B 50 (1994) 17953.
[16] J.M. Farmer, L.A. Boatner, B.C. Chakoumakos, M.H. Du, M.J. Lance, C.J. Rawn, J.C. Bryan, J. Alloy. Compd. 605 (2014) 63.
[17] J. Heyd, G.E. Scuseria, M. Ernzerhof, J. Chem. Phys. 118 (2003) 8207.
[18] J. Heyd, G.E. Scuseria, M. Ernzerhof, J. Chem. Phys. 125 (2006) 224106.
[19] B.P. Mandal, N. Garg, S.M. Sharma, A.K. Tyagi, J. Solid State Chem. 179 (2006) 1990.
[20] T. Hagiwara, H. Yamamura, H. Nishino, IOP Conf. Ser.: Mater. Sci. Eng. 18 (2011) 132003.